The physics of badminton

2015 New J. Phys. 17 063001

(http://iopscience.iop.org/1367-2630/17/6/063001)

New Journal of Physics
The open access journal at the forefront of physics

Deutsche Physikalische Gesellschaft DPG
IOP Institute of Physics

Published in partnership with: Deutsche Physikalische Gesellschaft and the Institute of Physics

OPEN ACCESS

RECEIVED
15 December 2014

REVISED
20 March 2015

ACCEPTED FOR PUBLICATION
31 March 2015

PUBLISHED
1 June 2015

PAPER

The physics of badminton

Caroline Cohen[1], **Baptiste Darbois Texier**[1], **David Quéré**[2] **and Christophe Clanet**[1]

[1] LadHyX, UMR 7646 du CNRS, Ecole Polytechnique, 91128 Palaiseau Cedex, France
[2] PMMH, UMR 7636 du CNRS, ESPCI, 75005 Paris, France

Keywords: physics of badminton, shuttlecock flight, shuttlecock flip, badminton trajectory

Abstract

The conical shape of a shuttlecock allows it to flip on impact. As a light and extended particle, it flies with a pure drag trajectory. We first study the flip phenomenon and the dynamics of the flight and then discuss the implications on the game. Lastly, a possible classification of different shots is proposed.

Introduction

History

The first games important to the creation of badminton were practised in Asia 2500 yr BC [1]. Soldiers played *ti-jian-zi*, which consisted of exchanging with their feet a shuttle generally made of a heavy leather ball planted with feathers (figure 1(a)). This game is now called *chien-tsu* and is practised with modern shuttles as shown in figure 1(b). Rackets were introduced for the first time in Japan with *hagoita* (figure 1(c)). During this period, shuttles were composed of the fruits of the Savonnier tree, which look like beans and were again furnished with feathers. Contemporary badminton is a racket sport originating from the Indian game *tomfool*, modified by British colonials, and played with a feathered shuttlecock and a racket made with strings, as attested by the painting of Jean-Siméon Chardin, reproduced in figure 1(d).

The modern game

Badminton is played either by two opposing players (singles) or two opposing pairs (doubles). Each player (or team) stands on opposite halves of a rectangular court which is 13.4 meters long, 5.2 meters wide and divided by a 1.55 meter-high net (figure 2(a)). Players score points by striking a shuttlecock with their rackets (a typical racket is shown in figure 2(b)) so that it passes over the net and lands in the opponent's half-court. Each side may strike the shuttlecock only once before it passes over the net. A rally ends once the shuttlecock has hit the floor or a player commits a fault. The shuttlecock is a feathered (or, in uncompetitive games, plastic) projectile. It is made of 16 goose feathers planted into a cork (figure 2(c)). This object weighs $M = 5$ g, its length is $L = 10$ cm and its diameter is $D = 6$ cm. Shuttlecocks have a top speed of up to 137 m s^{-1} [2]. Since the projectile flight is affected by the wind, competitive badminton is played indoors. Since 2008, all the finals of the Olympic Games and the World Championships have been contested by Lin Dan (China) and Lee Chong Wei (Malaysia). Looking at those finals, one observes that a typical game lasts about one hour (20 min by set), each rally lasts on average about 10 s with typically 10 exchanges. Badminton strategy consists of performing the appropriate shuttlecock trajectory, which passes over the net, falls in the limit of the court and minimizes time for the opponent reaction.

The state of the art

The trajectories of shuttlecocks have been extensively studied with experimental, theoretical and numerical approaches. Cooke recorded the trajectories of different shuttlecocks in the court and compared them to numerical simulations [3]. The aerodynamics of several shuttlecocks was studied in a wind tunnel by Cooke and Firoz [4, 5]. They measured the air drag $F_D = \rho S C_D U^2/2$ exerted by air on a shuttlecock (where ρ is the air density, $S = \pi (D/2)^2$ the shuttlecock cross-section and U its velocity) and showed that the drag coefficient C_D is approximatively constant for Reynolds numbers ($Re = DU/\nu$, with ν the air kinematic viscosity) between 1.0×10^4 and 2.0×10^5. For commercial shuttlecocks, C_D varies between 0.6 and 0.7 depending on the design

Figure 1. (a) Engraving of a ti-jian-zi game extracted from *Le Tour du Monde: Nouveau Journal des Voyages* written by Edouard Charton in 1860. (b) Shuttle used in chien-tsu. (c) Drawing of *Three Beauties Playing Battledore and Shuttlecock* by Utagawa Toyokuni in 1800. (d) *La Fillette au Volant* by Jean-Siméon Chardin in 1741.

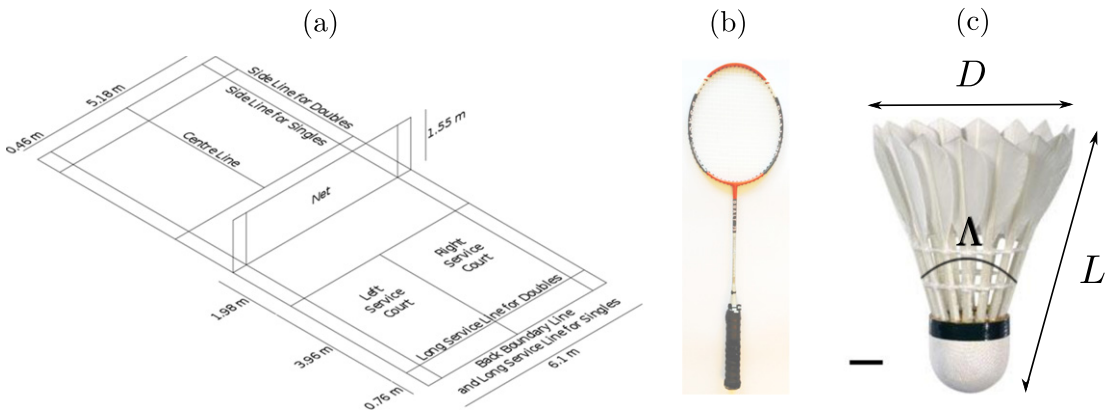

Figure 2. (a) Sketch of a badminton court. (b) A badminton racket. (c) An example of a feathered shuttlecock. The dark line indicates 1 cm. This image has been obtained by the author from the Wikipedia website and the owner of the copyright in the image is unclear. Accordingly, to the extent that the law allows, IOP Publishing disclaims any liability that any person may suffer as a result of accessing, using or forwarding the image and permission should be sought before using or forwarding the image from Wikipedia and/or the copyright owner. This image was made available on Wikipedia under a creative commons CC BY SA 3.0 licence.

of the skirt. Wind tunnel measurements also reveal that there is no lift force on a shuttlecock when its axis of symmetry is aligned along the velocity direction. A synthesis of data collected in the court and wind tunnels has been done by Chan [6]. Shuttlecock trajectories have been calculated by Chen [7], and Cohen *et al* [8] proposed an analytical approximation for the range of projectiles submitted to weight and drag at high Reynolds number. Nevertheless, the peculiarities of shuttlecocks such as their conical shape and flipping properties have rarely been discussed [9]. For instance, the observation of impacts with a racket (figure 3) reveals a dynamics specific to badminton: shuttlecocks fly with the nose ahead so that they can be hit on the cork by each player, which requires the shuttlecock to flip after each racket impact.

The questions we address in this work are: what makes the shuttlecock flight unique, and how does it influence the badminton game? In the first section, we study the 'versatile' behavior of a shuttlecock. The characteristic times associated with the motion are measured, and we develop an aerodynamical model to predict them. The second part concerns trajectories at the scale of the court, that is, for clear strokes. In this section, we study how the flight of a shuttlecock depends on its characteristics (mass, composition and geometry) and on the fluid parameters (density, temperature and humidity). Finally, we discuss in the third section how the shuttlecock flight influences the badminton game in terms of techniques, strategies and rules.

1. Flips

1.1. Observations

Different sequences of the flip of a shuttlecock are recorded using a high speed video camera (figure 3). After contact with the racket (typical time of 1 ms), it takes typically 20 ms for the projectile to flip. Then, the shuttlecock axis undergoes damped oscillations until it aligns along the velocity direction **U**. The projectile never

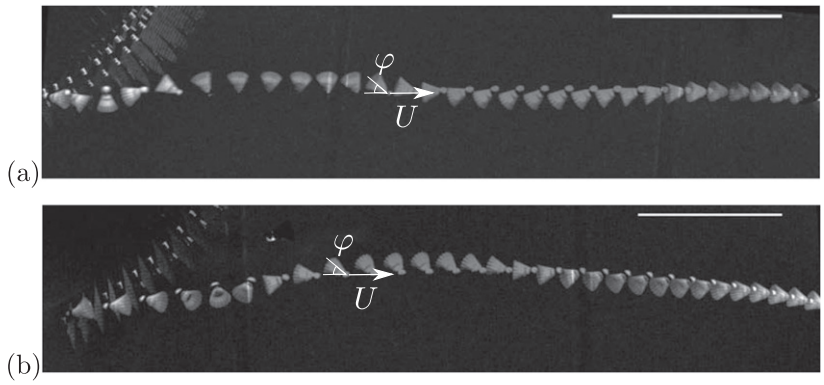

Figure 3. Chronophotographies of shuttlecocks after an impact with a racket, showing the time evolution of the angle φ between the shuttlecock orientation and its velocity **U**. White lines indicate 50 cm. (a) The time interval between each position is 5 ms, the shuttlecock initial velocity is $U_0 \approx 18.6$ m s^{-1} and its initial angular velocity is $\dot{\varphi}_0 = 206$ rad s^{-1}. (b) Time interval between each position is 6.5 ms, the shuttlecock initial velocity is $U_0 \approx 10.4$ m s^{-1} and its initial angular velocity is $\dot{\varphi}_0 = 28$ rad s^{-1}.

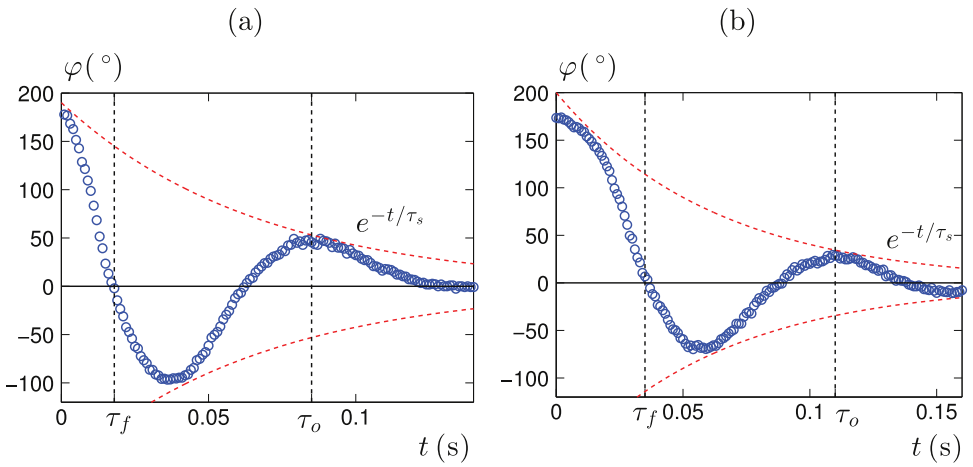

Figure 4. Time evolution of the angle φ between the shuttlecock axis of symmetry and its velocity **U**. Measurements correspond to experiments shown in figure 3. $t = 0$ is the time when the shuttlecock impacts the racket. Experimental data (blue dots) are bounded by an exponential envelope (red dashed lines). (a) The shuttlecock initial velocity is $U_0 \approx 18.6$ m s^{-1} and its initial angular velocity is $\dot{\varphi}_0 = 206$ rad s^{-1}. (b) The shuttlecock initial velocity is $U_0 \approx 10.4$ m s^{-1} and its initial angular velocity is $\dot{\varphi}_0 = 28$ rad s^{-1}.

performs a complete turn. In figure 3(a), the flip lasts four time intervals, which corresponds to 15 ms. The oscillating time of the shuttlecock direction is estimated as 80 ms. After 130 ms, the shuttlecock axis of symmetry is aligned along the velocity direction. When the hit intensity decreases, the dynamics of the shuttlecock slows down. Figure 3(b) shows the same shuttlecock leaving the racket at a velocity two times smaller than the previous one. The flipping time increases to 35 ms, the oscillating time lasts about 120 ms and the stabilizing time is estimated as 180 ms.

Such movies allow us to measure the angle φ between the shuttlecock axis and the velocity direction, as defined in figure 3. A typical example of the time evolution of φ is plotted in figure 4. Such graphs highlight the three characteristic times introduced earlier. The first one is the flipping time τ_f needed for φ to vary from 180° to 0°. The second one, denoted as τ_o, is the pseudo-period of oscillations. The third one is the stabilizing time τ_s, which corresponds to the damping of the oscillations (red dashed lines in figure 4). The purpose of this section is to understand this complex dynamics.

1.2. Flip model

In order to understand the shuttlecock behavior after impact, it is necessary to evaluate the forces applied to it, namely weight and aerodynamic pressure forces. These latter reduce to drag, the application point of which being the pressure center, where the aerodynamic torque vanishes [10]. Its location depends on the pressure profile around the projectile. If this profile is constant around the projectile, the aerodynamic center is the centroid of the object. Since the mass as a function of axial distance is non-homogeneous in a shuttlecock, the

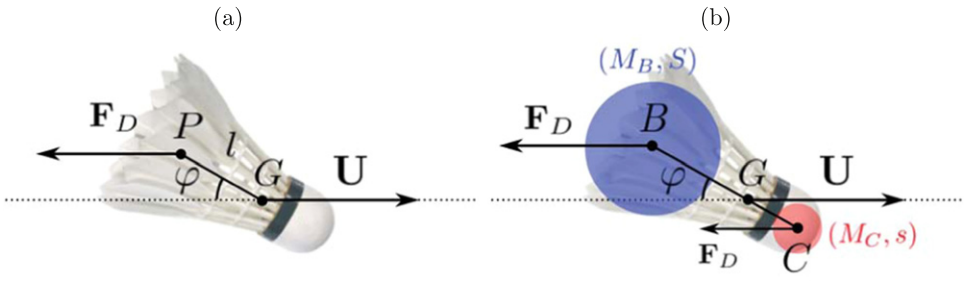

Figure 5. (a) Drag force $\mathbf{F}_D$ applied on a shuttlecock whose direction forms an angle φ with the velocity $\mathbf{U}$. (b) Model system composed of a sphere of large section S and mass M_B, which stands for the skirt, and a sphere of small section s and large mass M_C, which represents the cork.

center of gravity is closer to the cork and it differs from the center of pressure. Using numerical simulations, Cooke estimates that the distance l between the center of mass and center of pressure is about 3.0 cm [3]. The sketch in figure 5(a) highlights the effect of the drag $\mathbf{F}_D$ on an inclined shuttlecock. The aerodynamic drag applies a torque in a way opposite to the projectile velocity $\mathbf{U}$ and stabilizes the cork (corresponding to $\varphi = 0$).

Since the versatile behavior of a shuttlecock arises from the non-coincidence between its center of mass and center of pressure, we model the object with two spheres. The first one stands for the skirt of mass M_B and large cross-section S positioned in B, and the second one represents the cork of mass M_C and smaller cross-section s placed in C (figure 5(b)). The shuttlecock characteristics are condensed in a heavy small cork and a large light skirt. A torque balance around G provides the following equation in the realistic limit $SM_C \gg sM_B$:

$$\ddot{\varphi} + \frac{\rho S C_D U}{2M_B\left(1 + M_B/M_C\right)}\dot{\varphi} + \frac{\rho S C_D U^2}{2(M_C + M_B) l_{GC}} \sin\varphi = 0 \tag{1}$$

where C_D is the drag coefficient of a sphere and l_{GC} the distance between the points G and C ($l_{GC} = M_B/M_C\ l_{BC}$). The calculation leading to equation (1) is detailed in appendix A. This second order differential equation for φ is one of a damped oscillator. The square of pulsation $\omega_0^2 = \rho S C_D U^2/2\, M l_{GC}$ corresponds to the stabilizing torque generated by the aerodynamic drag (figure 5(b)). The damping term, $1/\tau_s = \rho S C_D U/2M_B(1 + M_B/M_C)$, results from the drag associated with the orthoradial movement of the shuttlecock as φ varies. The different characteristic times arising from (1) can finally be compared to the data.

1.2.1. Flipping time

Experiments show that the flipping time is smaller than the stabilizing time. This remark leads one to neglect the damping term $\dot{\varphi}/\tau_s$ in equation (1). In this limit, the equation of motion can be integrated with the initial conditions $\varphi(t = 0) = \pi$ and $\dot{\varphi}(t = 0) = \dot{\varphi}_0$, which yields:

$$\dot{\varphi}^2 = \dot{\varphi}_0^2 + 2\,\omega_0^2(1 + \cos\varphi). \tag{2}$$

Hence, the flipping dynamics of the shuttlecock depends on the pulsation ω_0 and initial angular velocity $\dot{\varphi}_0$. In our experiments, we have $M_C = 3.0$ g, $M_B = 2.0$ g and $S = 28$ cm^2, and we assume $C_D = 0.44$ and $l_{GC} = 2.0$ cm, as determined by Cooke [4]. Together with the air density $\rho = 1.2$ kg m^{-3}, we get a pulsation $\omega_0 \simeq 10$ rad s^{-1}, for $U = 10$ m s^{-1}. If $\dot{\varphi}_0 \gg \omega_0$, equation (2) reduces to $\dot{\varphi}(t) = \dot{\varphi}_0$ and the flipping time, defined as $\varphi(\tau_{f\ th}) = 0$, becomes:

$$\tau_{f\ th} = \frac{\pi}{\dot{\varphi}_0}. \tag{3}$$

This limit corresponds to the experiments reported in figures 3(a) and 4(a) where $\dot{\varphi}_0 = 206$ rad s^{-1} and $\omega_0 = 23$ rad s^{-1}. If the condition $\dot{\varphi}_0 \gg \omega_0$ is not satisfied, equation (2) must be integrated numerically using: $\tau_{f\ th} = \int_{\pi}^{0} d\varphi \Big/ \sqrt{\dot{\varphi}_0^2 + 2\omega_0^2(1 + \cos\varphi)}$, as for the data reported in figures 3(b) and 4(b). The determination of U_0, φ_0 and $\dot{\varphi}_0$ for the experiments shown in figure 3(a) and (b) allows us to estimate the flipping time. We find $\tau_{f\ th-a} = 15$ ms and $\tau_{f\ th-b} = 42$ ms for experiments (a) and (b). These predictions are close to the experimental values of $\tau_{f\ exp-a} = 16$ ms and $\tau_{f\ exp-b} = 39$ ms. Moreover, we can look at the flipping time $\tau_{f\ \mathrm{exp}}$ of a shuttlecock submitted to impacts of various intensities. For each impact, the initial rotational velocity

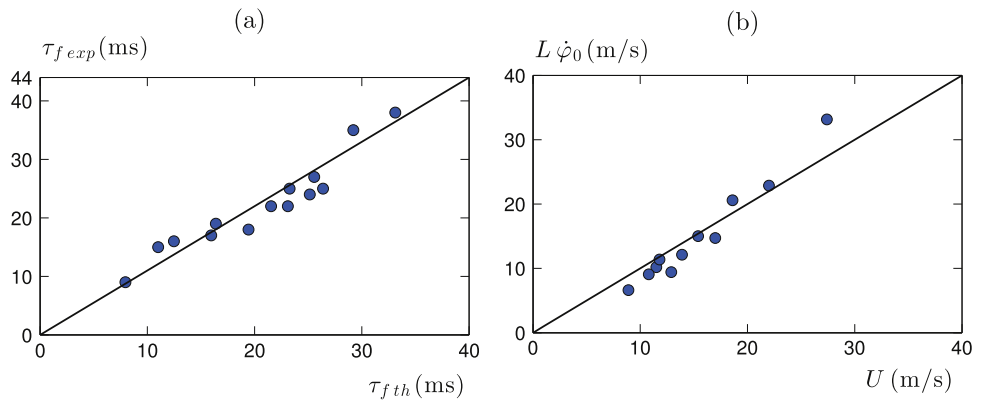

Figure 6. (a) Experimental flipping time $\tau_{f\ exp}$ as a function of the one $\tau_{f\ th}$ predicted by equation (2). (b) Experimental initial angular velocity $\dot{\varphi}_0$ times the skirt length L, as a function of the shuttlecock initial velocity U after its impact with a racket.

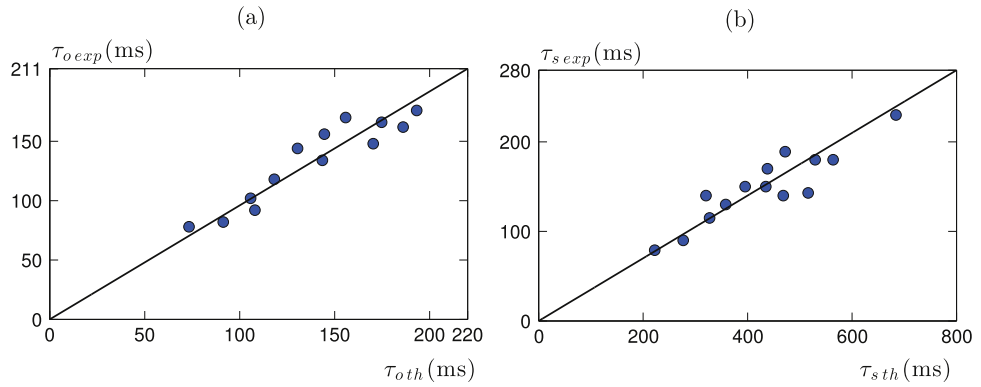

Figure 7. (a) Experimental oscillating time $\tau_{o\ exp}$ as a function of the predicted one $\tau_{o\ th}$, determined from equation (4) including the measured value of the shuttlecock velocity U. (b) Experimental stabilizing time $\tau_{s\ exp}$ as a function of the predicted one $\tau_{s\ th}$ estimated by the way of relation (5).

$\dot{\varphi}_0$ and shuttlecock speed U are measured. Figure 6(a) compares the experimental flipping time $\tau_{f\ exp}$ with the theoretical one $\tau_{f\ th}$ predicted by solving equation (2).

All the data (blue dots) are distributed around a line of slope 1.1. Figure 6(b) highlights the dependency between the initial angular velocity $\dot{\varphi}_0$ and its initial velocity U. For a standard impact, the two initial conditions given to a shuttlecock are thus not independent.

1.2.2. Oscillating time

The oscillating time of a shuttlecock can also be predicted by equation (1). By considering typical values of the characteristics of a shuttlecock, we estimate the quantity $1/\omega_0\tau_s = \sqrt{2\,M\rho SC_D l_{GC}}/2M_B(1 + M_B/M_C) \simeq 0.04$. This leads one to consider low damped oscillations where the oscillating time can be expressed as $\tau_o = 2\pi/\omega_0$. This approximation provides:

$$\tau_{o\ th} \simeq 2\pi\frac{\sqrt{\mathcal{L}\ l_{GC}}}{U} \tag{4}$$

where $\mathcal{L} = 2\,M/\rho SC_D$. Using the previous values for shuttlecock characteristics and the initial velocities in experiments shown in figures 3(a) and (b), we estimate the oscillating times using relation (4). This provides $\tau_{o\ th-a} = 102$ ms and $\tau_{o\ th-b} = 183$ ms for the experiments (a) and (b), which nicely compares to the data $\tau_{o\ exp-a} = 92$ ms and $\tau_{o\ exp-b} = 168$ ms. Moreover, we can inspect experimentally the oscillating time $\tau_{o\ exp}$ of a given shuttlecock submitted to impacts of various intensities. For each impact, the shuttlecock speed U and its oscillating time are measured. Figure 7(a) shows that the experimental flipping time $\tau_{o\ exp}$ agrees with $\tau_{o\ th}$, the one predicted by equation (4).

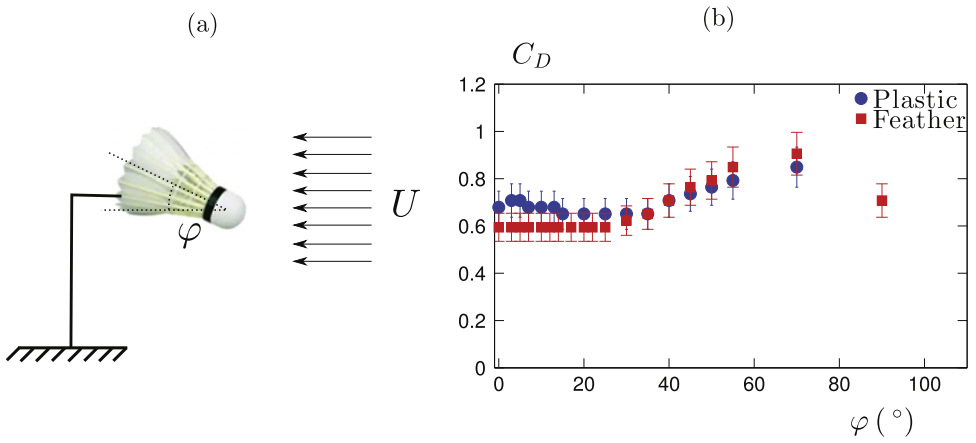

Figure 8. (a) Sketch of the setup used to measure the drag coefficient of a shuttlecock in a wind tunnel as a function of its orientation with the air flow. (b) Drag coefficients of a plastic (blue dots) and a feathered (red squares) shuttlecock as a function of its orientation in the air flow. Measurements have been done with a wind velocity $U = 14.5$ ms^{-1} and non-spinning projectiles.

1.2.3. Stabilizing time

The stabilizing time is experimentally determined to be about one hundred milliseconds (figure 3) and it appears in equation (1) through the damping term $\dot{\varphi}/\tau_s$. According to the previous model, it can be expressed as:

$$\tau_{s\,th} = \frac{2M_B\left(1 + M_B/M_C\right)}{\rho S C_D U} = \frac{M_B}{M_C}\frac{\mathcal{L}}{U}. \tag{5}$$

For typical orders of magnitude implied in badminton ($U = 20$ m s^{-1}), this relation provides $\tau_s \sim 0.3$ s. We can look at the evolution of the stabilizing time with the shuttlecock velocity for different impacts. Figure 7(b) shows the stabilizing time as a function of the one predicted by equation (5). All the data (blue dots) collapse on a line of slope 0.4. The fact that the slope is lower than unity may come from the approximation of a drag coefficient independent of the shuttlecock orientation. Actually, the shuttlecock drag coefficient increases with the orientation angle φ as shown in figure 8(b). This phenomenon, which is not taken into account in the model, tends to reduce the calculated stabilizing time.

1.3. On the shape of a shuttlecock

We now discuss how the shuttlecock geometry influences its flipping dynamics, which ideally might explain why a shuttlecock opening angle Λ close to 45 °was selected (figure 2(c)). In order to answer this question, shuttlecock prototypes have been constructed. They are made with a dense iron ball and a light plastic skirt (figure 9(a)). The characteristics of these prototypes (length L, diameter D, mass M and opening angle Λ) can be easily varied. For each one, the flipping dynamics was captured and analyzed in a free fall experiment where the shuttlecock was released upside down without initial velocity. These experiments were conducted in a water tank in order to reduce the length scales. The Reynolds number corresponding to the flow is also reduced but it stays in the regime of high Reynolds number ($Re > 10^3$) where fluid effects are described by the same laws. Figure 9(b) shows a chronophotograph of a prototype flipping during its fall in water. We performed experiments with given mass M and diameter D, but different opening angles Λ between 10° and 160°. The evolution of $\tau_{f\ \mathrm{exp}}$ and $\tau_{s\ \mathrm{exp}}$ with Λ is reported in figure 9(c). The graph shows the existence of an optimal opening angle for which the flipping and stabilizing times are minimal.

The dependency of τ_o and τ_s with Λ can be understood qualitatively. For small opening angles, the shuttlecock is elongated and the skirt has a high momentum of inertia. The object is difficult to set in motion and the characteristic times are long. In the opposite case (large Λ) the shuttlecock is short and l is small as the stabilizing torque resulting from the drag force. This situation also corresponds to large values of flipping and stabilizing times. Between these two regimes, there is a range of opening angles for which the flipping motion is faster. Real shuttlecocks seem to belong to this family of intermediate opening angles that rapidly flip.

The basic model developed previously for shuttlecocks can be applied to any object which have a distinct center of mass and center of pressure.

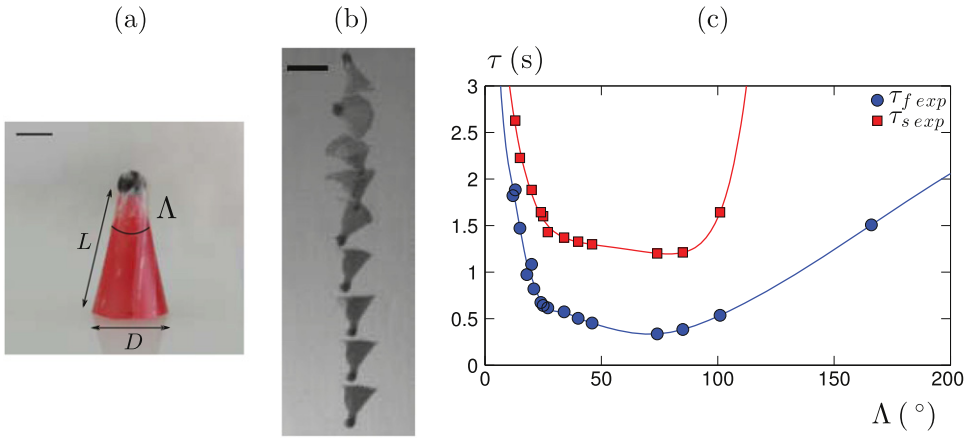

Figure 9. (a) Prototype of a shuttlecock made with a dense iron ball and a light plastic skirt. The dark line indicates 1 cm. (b) Chronophotography of a prototype launched upside down without initial velocity in a water tank. Snapshots are separated by 160 ms and the bar indicates 2 cm. (c) Flipping (blue dots) and stabilizing (red squares) times are plotted as a function of the shuttlecock opening angle Λ. Shuttlecocks have a mass $M = 2.2$ g and a section $S = \pi (D/2)^2 = 12.4$ cm^2.

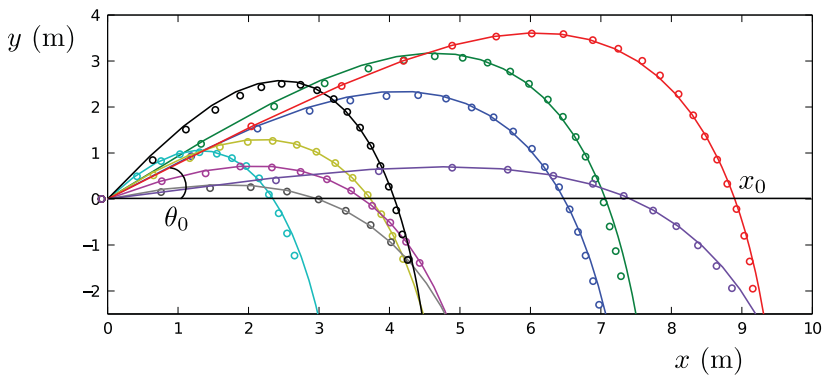

Figure 10. Comparison between the observed trajectories (circles) and trajectories calculated with a pure drag equation and $\mathcal{L} = 4.6$ m (solid line) for different initial conditions: $U_0 = 19.8$ m s^{-1} and $\theta_0 = 39°$ (blue); $U_0 = 24.7$ m s^{-1}, $\theta_0 = 44°$ (green); $U_0 = 6.8$ m s^{-1}, $\theta_0 = 55°$ (cyan); $U_0 = 9.7$ m s^{-1}, $\theta_0 = 44°$ (yellow); $U_0 = 9.5$ m s^{-1}, $\theta_0 = 30°$ (light-purple); $U_0 = 9.6$ m s^{-1}, $\theta_0 = 18°$ (gray); $U_0 = 13.4$ m s^{-1}, $\theta_0 = 58°$ (black); $U_0 = 37.6$ m s^{-1}, $\theta_0 = 38°$ (red); $U_0 = 32.3$ m s^{-1}, $\theta_0 = 12°$ (dark-purple).

2. High clears

2.1. Trajectories

We now discuss the global trajectory of a shuttlecock. The equation of motion for such a projectile is $M\frac{d\mathbf{U}}{dt} = M\mathbf{g} - \frac{1}{2}\rho S C_D U\mathbf{U}$. The trajectory depends on the initial conditions U_0, θ_0 and on a characteristic length $\mathcal{L} = 2M/\rho S C_D$ called the aerodynamic length. Considering $M = 5.0$ g, $\rho = 1.2$ kg m^{-3}, $S = 28$ cm^2 and $C_D = 0.65 \pm 0.05$ (determined in a wind tunnel), we get $\mathcal{L} = 4.6$ m. This value allows us to evaluate the projectile terminal velocity in free fall, $U_\infty = \sqrt{g\mathcal{L}} = 6.7$ m s^{-1}, which corresponds to the steady state $d\mathbf{U}/dt = \mathbf{0}$. Numerical solutions of the equation of motion for various initial conditions are plotted in figure 10 with solid lines. These trajectories are compared with experimental ones of the same initial conditions U_0 and θ_0 (see dots in figure 10). The time step between two positions is 100 ms.

One observes the superimposition of numerical and experimental trajectories. This agreement validates the assumptions of constant C_D (and S) along the shuttlecock trajectory, as also observed by Phomsoupha *et al* [11]. The equation of motion for shuttlecocks has an analytical solution [8]. This solution leads to an approximate expression for the range x_0 of the projectile, defined as the position on the horizontal axis where the particle returns to its initial height (figure 10):

$$x_0 = \frac{\mathcal{L}}{2}\cos\theta_0 \ln\left(1 + 4\frac{U_0^2}{g\mathcal{L}}\sin\theta_0\right). \quad (6)$$

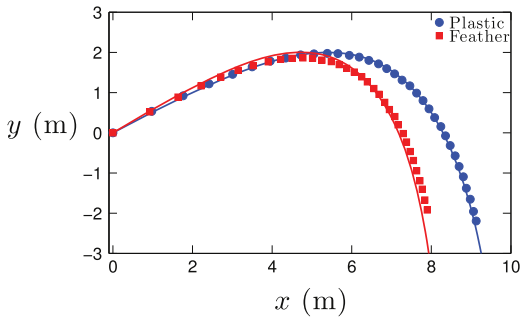

Figure 11. Plastic and feathered shuttlecock trajectories obtained with the same initial conditions, θ_0 and U_0. Blue and red dots are used for plastic or feathered projectiles respectively. Solid lines are numerical solutions of the equation of motion using the same initial conditions as in experiments. The aerodynamic length is determined for each shuttlecock from wind tunnel measurements.

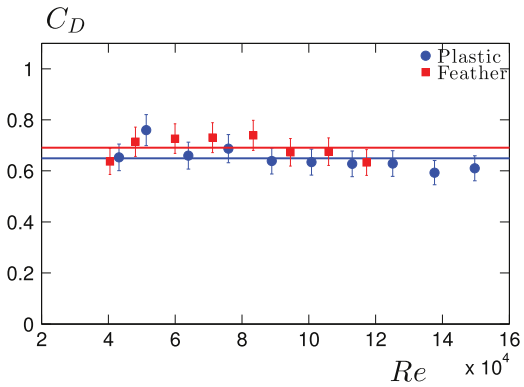

Figure 12. Drag coefficient ($C_D = 2F_D/\rho\pi\,(D/2)^2U^2$) as a function of the Reynolds number ($Re = DU/\nu$). Blue dots stand for plastic shuttlecocks whereas red squares are used for feathered projectiles. Solid lines show the mean value of the drag coefficient in each case.

If $U_0 \ll U_\infty = \sqrt{g\mathcal{L}}$, equation (6) reduces to the parabolic range $x_0 = U_0^2 \sin 2\theta_0/g$. In the opposite case ($U_0 \gg U_\infty = \sqrt{g\mathcal{L}}$), we observe a logarithmic dependency of x_0 with the initial velocity: the range virtually saturates at a distance scaling as $\mathcal{L}$. In badminton, the initial launching velocity U_0 is often much larger than U_∞ and players can feel the saturation of the range with initial velocity. In this regime, x_0 highly depends on shuttlecock and air properties through the aerodynamic length $\mathcal{L}$. In the following, the influence of the shuttlecock and fluid characteristics on trajectories is studied.

2.2. Difference between plastic and feather shuttlecocks

Shuttlecocks are usually classified in two categories, namely plastic and feathered. In order to understand the difference between both types, we observed their trajectories. Figure 11 reports two shuttlecock trajectories with the same initial conditions but with a different kind of projectile.

With the same initial angle and velocity, the range is larger for plastic than for feathered shuttlecocks. This increase is about one meter, which represents 10% of the total range. This phenomenon is observed on a large variety of plastic and feathered shuttlecocks [3]: both projectiles can be distinguished by their aerodynamic lengths. Parameters influencing $\mathcal{L}$ are determined, such as drag coefficients measured in a wind tunnel, and results are plotted in figure 12.

Since C_D is independent of the Reynolds number, we consider its mean value. For the feathered projectile, it is $C_{Df} = 0.65 \pm 0.05$ whereas we have for the plastic one $C_{Dp} = 0.68 \pm 0.05$. The exposed section $S = \pi\,(D/2)^2$ is equal to 28 cm^2 for both shuttlecocks. The shuttlecock's mass is $M_f = 5.0$ g for the feathered one and $M_p = 5.3$ g for the plastic. Combining all these data, we estimate the aerodynamic length for each kind of shuttlecock: $\mathcal{L}_f = 4.04$ m and $\mathcal{L}_p = 4.48$ m. We solve numerically the equation of motion including these values and plot the resulting trajectories in figure 11 with solid lines. Numerical trajectories correspond to experimental ones and predict the range for both kinds of shuttlecock. Trajectories mainly differ because of the difference in aerodynamic length between the two projectiles, a difference itself due to the larger mass of a plastic

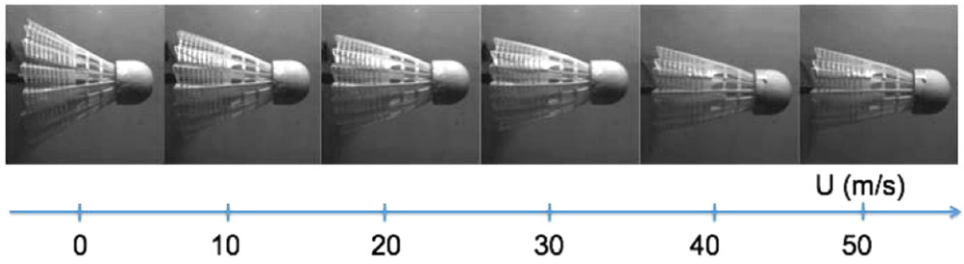

Figure 13. Deformation of a plastic shuttlecock with a cut skirt, submitted to an increasing air flow velocity.

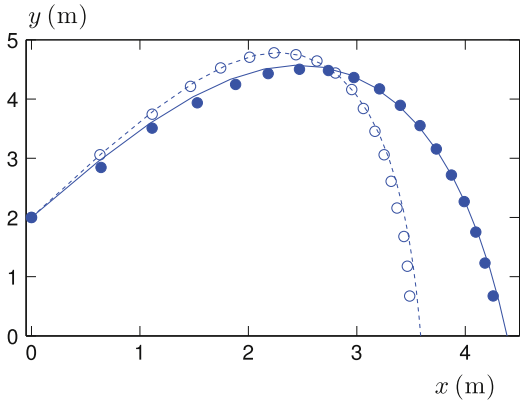

Figure 14. Comparison between the trajectory of a standard plastic shuttlecock (full blue dots) and the one of a cut shuttlecock (empty blue dots). The time interval between two positions is 100 ms. The blue solid line shows the solution of the equation of motion with the same initial conditions and the same properties of a standard shuttlecock while the dashed line shows this solution after taking into account the modification of the cross-section of the projectile measured in a wind tunnel (figure 13).

shuttlecock compared to a feathered one. It is practically not very easy to reduce the mass of a plastic projectile while keeping its robustness and price unchanged, which explains why the two masses are different.

Experienced players prefer to play with a fragile feathered shuttlecock than with a cheaper and more resistant plastic one. This can be understood by the fact that feathered projectiles may have faster initial velocities without exiting the court, owing to their smaller aerodynamic length. Using feathered shuttlecocks, a player can hit a smash at a higher speed, which allows less time for the opponent to react.

According to experienced players, the trajectories of feathered shuttlecocks are more 'triangular', as indeed seen in figure 11. Players' feelings about the triangular nature of the trajectory may come from the curvature at the top $\left(\frac{d\theta}{ds}\right)_{\theta=0}$, which is inversely proportional to $\mathcal{L}$ and independent of the initial velocity U_0. As a consequence, feathered trajectories are indeed more curved at the top than plastic ones.

As the shuttlecock geometry is critical for the badminton game, we have imagined a way to approach the pure triangular trajectory. The skirt rigidity of a plastic shuttlecock is reduced by cutting it longitudinally (first image in figure 13). Figure 13 shows that increasing air flow reduces the cross-section S of the projectile by a factor 2 as the flow velocity increases from 0 m s^{-1} to 50 m s^{-1}.

Figure 14 compares the trajectory of a cut shuttlecock with the one observed for a standard plastic projectile. For similar initial conditions, the skirt deformability indeed induces a modified trajectory which is more triangular than the normal one. The fact that the shuttlecock with a cut skirt has a lower range means that the increase of its cross-section at low speed predominates over its reduction at high velocity.

2.3. Shuttlecock rotation

Shuttlecocks are not exactly symmetric with respect to their axis because feathers are superimposed one over another. This asymmetry also exists for plastic models, and it implies that a shuttlecock rotates around its axis when placed into an air flow [12]. This section quantitatively describes this effect shown in figure 15(a). Considering that the behavior of a feather is similar to the one of a thin plate in an air flow, the fluid force is perpendicular to the object and in a direction opposite to its velocity. Forces exerted on each feather (as

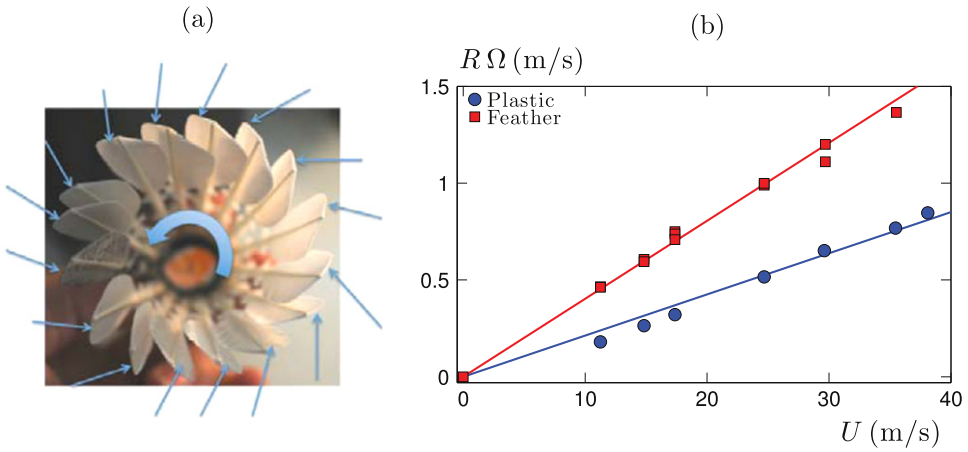

Figure 15. (a) Sketch indicating the rotation of a shuttlecock moving with the cork ahead. Thin blue arrows indicate the drag force on each feather. (b) Rotation velocity $R\ \Omega$ as a function of the translation speed U for a plastic (blue dots) and a feathered shuttlecock (red squares).

represented in figure 15(a) with blue arrows) create a torque which puts a projectile into rotation so that feathers rip through air.

Shuttlecocks rotate at a velocity such that this torque is balanced by air resistance. The rotational velocity Ω is measured as a function of the projectile speed U, as shown in figure 15(b). The graph reveals a linear correlation between $R\ \Omega$ and U, and differences between plastic and feather rotational velocities. Whereas the slope of the linear trend is equal to 0.02 for the plastic shuttlecock, the one for the feathered projectile is twice as large.

The link between the rotational and linear velocity of a shuttlecock can be understood by writing the balance between the propulsive and friction torques applied on a feather:

$$\rho S_p \sin(\Lambda/2)\ \sin\beta\ \ \cos\beta\ U^2\ R \sim \rho S_p \sin(\Lambda/2) \tan\left(\frac{R\Omega}{U}\right) U^2\ R \tag{7}$$

where S_p is the feather surface area, Λ the opening angle and β the tilted angle of feathers resulting from their superimposition. Experimental observations show that $R\Omega \ll U$, which leads to the following relation:

$$R\ \Omega \sim \sin\beta\ \cos\beta\ U. \tag{8}$$

This approach predicts the linear dependency of rotational shuttlecock velocity with U. In addition, the factor between these two quantities is estimated as 0.06 for $\Lambda \approx 45°$ and $\beta \approx 4°$ and the model roughly captures the origin of rotation of a shuttlecock around its axis, and its amplitude. The effect of rotation on the flight can also be discussed. In a wind tunnel, we measured the drag coefficients of projectiles without rotation or free to rotate. The results are gathered in figure 16. Whatever the rotation, the drag coefficient is found to remain between 0.65 and 0.75. Considering the uncertainty of our experiments, we conclude that the rotation of a shuttlecock has no strong effect on the drag coefficient.

One may wonder whether rotation induces gyroscopic stabilization. Such a phenomenon happens if the angular momentum of the shuttlecock is high compared to the aerodynamic torque applied to it. It eventually leads to a non-zero value of the angle φ between the axis of the shuttlecock and its velocity direction along the trajectory. Figure 17 reports the time evolution of this angle along a high clear trajectory. Apart from the first flipping phase, the shuttlecock is never tilted compared to its velocity direction.

The fact that axial rotation does not lead to gyroscopic stabilization can be understood. On the one hand, the angular momentum of this object is $J\Omega^2$ where J is the moment of inertia of the shuttlecock relative to its axis of rotation and Ω the angular velocity. On the other hand, the aerodynamic torque scales as $\rho R^2 U^2 l$. Gyroscopic stabilization only occurs if we have $R\Omega/U \gg R^2\sqrt{\rho l/J}$. Using a pendular system, Cooke measured different shuttlecocks' moments of inertia and concluded that J is 1.2×10^{-6} kg m^{-2} [3]. Considering typical values ($l \simeq 3$ cm, $R \simeq 3$ cm and $\rho = 1.2$ kg m^{-3}), we deduce the following criterion for gyroscopic stabilization: $R\Omega/U \gg 0.1$. According to figure 15(b), this condition is not achieved when rotation is imposed by air flow and shuttlecock rotation along its axis does not stabilize it in a direction different to the velocity one. However, when the axis is not aligned with the air flow, the aerodynamic torque on the rotating object induces a precessing motion of period $\tau_p = 4\pi J\Omega/\rho S C_D U^2\ l$. The typical distance over which a shuttlecock follows precession is $U\tau_p \sim (J/\rho R^3\ l)(R\Omega/U)$. Considering typical values of the ratio $R\Omega/U$ (extracted from figure 15(b)) and the characteristics of a shuttlecock, we estimate that $U\tau_p$ is about 2 m for a plastic projectile and 4 m for a feathered

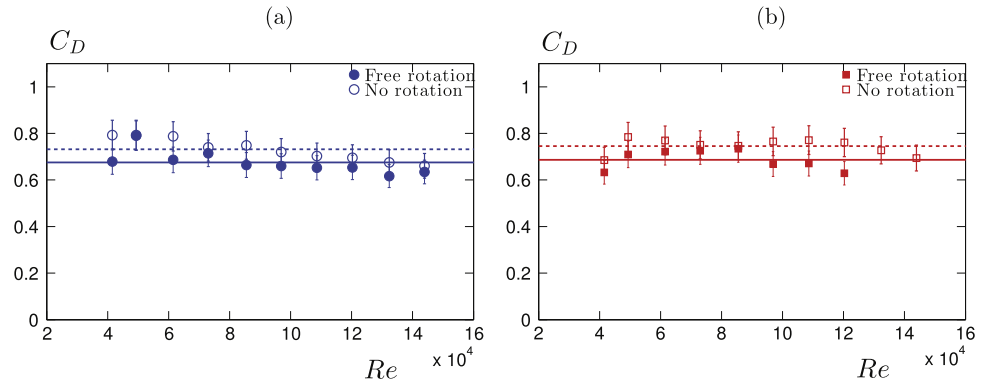

Figure 16. Shuttlecock drag coefficients ($C_D = 2F_D/\rho\pi\,(D/2)^2U^2$) as function of the Reynolds number ($Re = DU/\nu$) for projectiles free to rotate or not (full and empty symbols, respectively). (a) Plastic shuttlecock MAVIS 370. (b) Feathered shuttlecock.

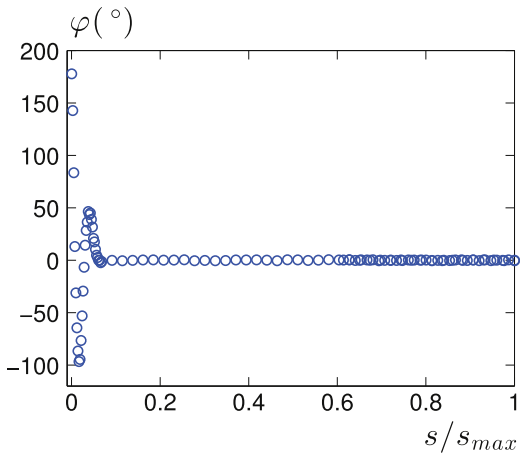

Figure 17. Plot of the experimental angle φ between the shuttlecock axis and its velocity as a function of the coordinate s of the shuttlecock along its trajectory divided by the curvilinear coordinate when the projectile reaches the floor ($s = s_{\max}$). The initial launching conditions correspond to a high clear: $U_0 = 26$ m s^{-1} and $\theta_0 = 56°$.

one. This difference leads to a smoother early path for the second case. This phenomenon may also contribute to the players' preference for feathered shuttlecocks.

Obayashi *et al* also investigated the effect of a shuttlecock rotation on to its skirt deflection [13]. They proved that the skirt enlargement due to the centrifugal forces is compensated by the effect of the aerodynamic drag. Thanks to rotation, shuttlecocks keep a constant cross-section.

3. Influence of the shuttlecock flight on the game

3.1. Flipping strokes

We discussed in section 1 how shuttlecocks flip after being impacted by a racket. Among the strokes used in badminton, we aim to determine which ones are influenced by this versatile motion. The flipping dynamics of a shuttlecock is sensitive to the players only if the stabilizing time τ_s compares to the total flying time τ_0. We plot in figure 18 the ratio τ_s/τ_0, where τ_s is deduced from relation (5), as a function of the horizontal traveled distance x_0 normalized by the court length L_{field}.

The graph reveals that there is only a small domain of the court ($x_0 \lesssim 0.25\,L_{field} = 3$ m) where players can receive a shuttlecock not yet aligned with its velocity direction. This situation only happens in the case of net drops. When a good player performs a net drop, his purpose is to delay the flip of the shuttlecock and let the skirt fly ahead. Then, the opponent cannot hit the cork of the shuttlecock and send it back properly. In practice, players perform tricks called 'spin in' and 'spin out', which consist of gently hitting the shuttlecock and simultaneously gripping the cork to maximize the initial spin $\dot{\varphi}_0$ positively or negatively. Relations (4) and (5)

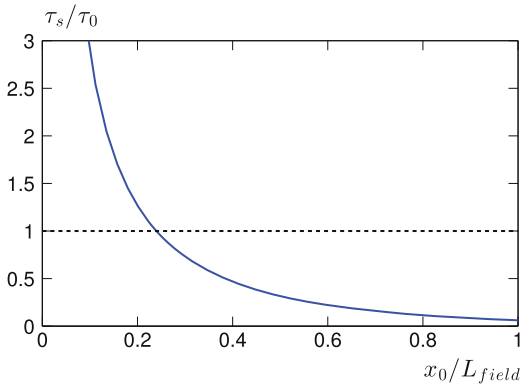

Figure 18. Ratio of the stabilizing time τ_s derived from expression (5) and the computed flying time τ_0 as a function of the horizontal range x_0 divided by the court length L_{field}. This plot is obtained for a shuttlecock of aerodynamic length $\mathcal{L} = 4.6$ m, initially launched at $y = 2$ m with an initial angle $\theta_0 = 15°$.

imply that a small initial velocity U_0, as employed in net drops, increases the shuttlecock oscillating and stabilizing times.

The criterion for having a shuttlecock turning several times on itself before stabilizing can be discussed quantitatively. This situation happens if the initial rotational kinetic energy, $(M_B l_{GB}^2 + M_C l_{GC}^2)\dot{\varphi}_0^2/2$, is larger than the depth of the potential energy well, $\rho S C_D U^2 l_{GC}/2$, imposed by the drag exerted on the skirt. One deduces that a shuttlecock does several turns before stabilizing if the initial angular velocity verifies $\dot{\varphi}_0 \gtrsim U\sqrt{\rho S C_D / l_{GC} M_B}$. For typical shuttlecocks, this relation becomes $L\dot{\varphi}_0/U \gtrsim 2.2$. In the case of standard impacts, we saw in figure 6(b) that $L\dot{\varphi}_0/U \sim 1$. This explains that shuttlecocks generally perform less than a complete turn after an impact with a racket. Only the 'spin in' or 'spin out' techniques allow one to outweigh this criterion and make the projectile turn several times before stabilizing with the nose ahead.

Apart from net drops, all other strokes have a stabilizing time shorter than the flying one. Thus the shuttlecock is always aligned with the velocity direction, corresponding to the trajectories studied in section 2.

3.2. Clear strokes

For clear strokes, section 2.1 shows that the range 'saturates' with the initial velocity at a maximal value which depends on the aerodynamical length $\mathcal{L}$. For the maximal initial speed ever recorded ($U_{max} = 137$ m s^{-1}), the shuttlecock maximum range x_{max} is 13.8 m [14]. This distance compares to the court length ($L_{field} = 13.4$ m), which implies that the projectile rarely leaves the field and may explain why the mean number of shots per rally (13.5) is so large in top level badminton competitions [15]. For comparison, this number falls to 3.5 in top level tennis competitions consistently with the fact that the maximum range of a tennis ball ($x_{max} = 66.9$ m) is much larger than the court length ($L_{field} = 24$ m).

3.3. A possible classification

Depending on players and shuttlecock positions, several kinds of stroke are used, as sketched in figure 19(a) [2]. Each stroke is characterized by a horizontal traveled distance x_0 and a flying time τ_0. We propose classifying badminton strokes in the diagram drawn in figure 19(b). On the x-axis, one finds the flying time τ_0 divided by the time of reaction τ_r of a player (τ_r is about 1 s for trained players). The y-axis shows the ratio between the horizontal traveled distance x_0 and the court length L_{field}. This diagram reveals that smashes, drives and net shots correspond to short flying time strokes, as opposed to clears, drops and lifts. The only stroke whose range is short compared to the court size is the net shot. A red color is used for killing shots of proportion larger than 10% (see table 1): all the short-time shots fall in this efficient category.

Badminton strategy consists in moving the opponent away from the court center using clear, drop or lift strokes before finishing the point with a rapid shot such as a smash or a net shot. This strategy impacts the strokes frequency as reported in table 1, which differentiates the killing shots from other ones. For clears, drops and lifts, the frequency of non-winning shots is much larger than the frequency of killing shots, which emphasizes that these shots are defensive or preparatory shots; this contrasts with drives, smashes and net shots which largely dominate the statistics of killing shots. Thus, ending a rally in badminton is mainly a question of flight duration.

3.4. Upwards and downwards strokes

Another way to classify the different strokes consists in noting the direction: the up-going family is composed of clear and lift, while the down-going family includes smash, drop and kill (which is an offensive shot hit from the

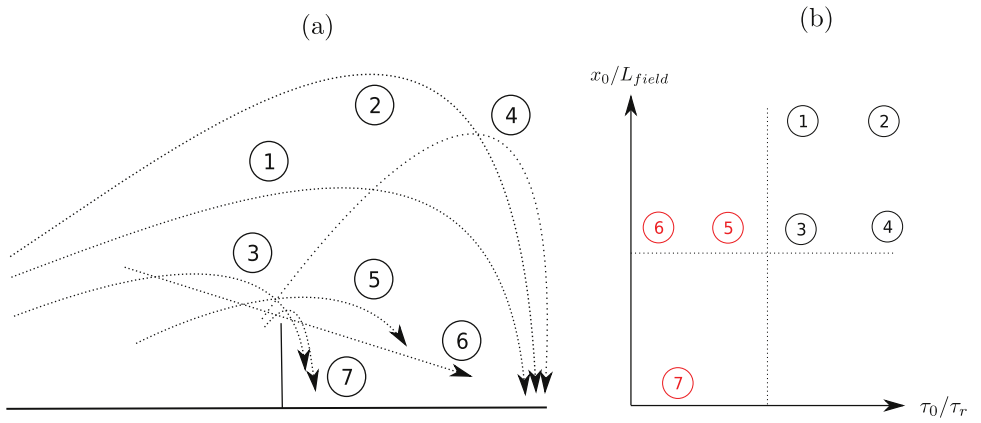

Figure 19. (a) Side view of the court showing the different shuttlecock trajectories during a game [2]. The clear can be an offensive stroke (1), moving the opponent back from the net or a defensive one (2), saving time to improve the player's position. Drops (3) and net shots (7) are slow, gentle shots that fall just behind the net into the opponent's forecast. A lift (4) is actually an underarm clear played from around the net area. This shot allows one to move the opponent to the back or to save time. The drive (5) is a line-drive shot parallel to the ground passing just over the net. The smash (6) is a fast ball with a sharp straight trajectory aimed either at the opponent's body or at the limits of the court. (b) Classification of badminton shots according to the ratio between the flying time τ_0 and the reaction time τ_r of the opponent, and to the ratio between the horizontal traveled distance x_0 and the court size L_{field}. Strokes highlighted in red have a frequency larger than 10% in killing shots (see table 1).

Table 1. Measurements of the frequency of different strokes (first column) as referenced in figure 19 for all playing shots (second column) and for killing shots (third column). Data are extracted from [16]. Strokes which are killing shots with a frequency larger than 10% are highlighted in bold, as also stressed in red in figure 19(b).

Strokes	Playing shots	Killing shots
Clear (1) & (2)	0.11	0.03
Drop (3)	0.07	0.03
Lift (4)	0.21	0.04
Drive (5)	0.14	**0.21**
Smash (6)	0.20	**0.54**
Net shots (7)	0.18	**0.15**
Serve	0.09	0

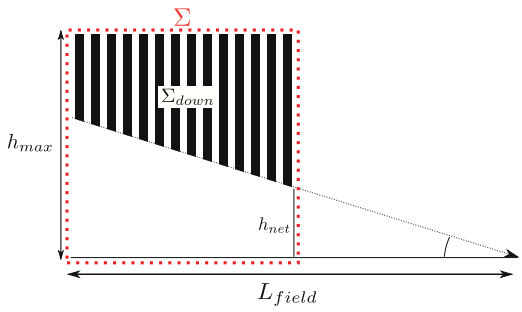

Figure 20. Sketch of a badminton court viewed from the side. In order to pass over the net, downward strokes have to be hit from the striped area.

net area and not reported in figure 19). The probability of each family can be approached with geometrical considerations. Due to the presence of a net, the down-going family must be hit high enough, as represented by the striped area in figure 20.

Considering that a badminton player can reach a maximum height h_{max}, that is, his/her own height (1.78 m for Lin Dan and 1.74 m for Lee Chong Wei), plus his/her jumping height (0.7 m for Lin Dan), plus the racket length (0.65 m), we estimate the total cross-sectional area Σ reachable by a player. Thus the ratio between the

Table 2. Measurements of the frequency of different downward strokes during the last four Olympic finals.

Downward strokes	Frequency
Smash	0.14
Drop	0.12
Kill	0.02
Total	0.28

down-going stroke area Σ_{down} and the total Σ is equal to $1 - \frac{3}{2}\frac{h_{net}}{h_{max}} = 0.26$, h_{net} being the height of the net. This ratio must be compared to the frequency of downward strokes. Analyzing the last four Olympic finals, Laffaye and Phomsoupha show that this frequency is equal to 0.28 (table 2), which is close to the ratio $\Sigma_{down}/\Sigma = 0.26$. One guesses that a change in the net height would modify this frequency and impact the characteristics of the game, such as the mean number of exchanges per rally and the mean number of points per unit time.

Conclusion

The dynamics of a shuttlecock and its influence on the badminton game have been questioned. The versatile behavior of a shuttlecock after impact arises from its non-homogenous mass as a function of axial distance. The cork being denser than the skirt, a shuttlecock has distinct centers of mass and pressure, and thus undergoes a stabilizing aerodynamic torque setting its nose ahead. The geometry of commercial shuttlecocks is empirically chosen to minimize flipping and stabilizing times. In practice, badminton players try to delay stabilization with net drops, in order to prevent the opponent from hitting the projectile correctly.

For other strokes, the stabilizing time is much shorter than the total flying time. In this limit, a shuttlecock is aligned with its velocity. Because this light particle experiences a large drag, its trajectory is nearly triangular [8] and it highly depends on the projectile properties. This explains why players carefully choose shuttlecocks as a function of skills and atmospheric conditions (see appendix B). Experienced players prefer shuttlecocks submitted to a slightly larger drag, such as feathered ones, in order to hit them violently without exiting the court. The difference in rotating speed between the two kinds of shuttlecock (plastic and feathered) also plays a role in this choice since a faster rotation of feather projectile limits its precession.

Beyond this study, many questions concerning the physics of badminton remain to be solved. For example, the impact dynamics of a shuttlecock with a racket is not considered in this paper. One may wonder if there is an optimal rigidity for the shaft and the strings to enhance the launching speed of a shuttlecock. Finally, the laws established for shuttlecock flights could be discussed with other projectiles having a non-homogeneous mass along their axis, such as air missiles [17] or dandelion achenes [18].

Acknowledgments

We thank G Laffaye and M Phomsoupha for precious help and advice concerning experiments, and badminton techniques and strategies. We are grateful to F Moisy for access to the wind tunnel of the FAST laboratory. We thank F Gallaire for unlimited interest concerning this subject. The authors acknowledge C and P Mace and J Careil for bringing our attention to badminton specificities. Finally we thank I Jobard for introducing us to the world of badminton referees.

Appendix A

Equation (1) describes the shuttlecock dynamics. The calculation leading to this equation from the model proposed in figure 5(b) is derived here. The velocity of point B in the reference frame along the vectors $\mathbf{e}_{GB}$ and $\mathbf{e}_{\varphi}$ is given by:

$$\mathbf{U}_B = \begin{pmatrix} -U\cos\varphi \\ U\sin\varphi + l_{GB}\,\dot{\varphi} \end{pmatrix}. \tag{9}$$

Table B1. Air density ρ as a function of its temperature T. For each condition, the shuttlecock aerodynamic length $\mathcal{L}$ is estimated with $M = 5.0$ g, $S = 28$ cm^2 and $C_D = 0.6$. The maximal range x_{max} is calculated for the maximal velocity recorded in a badminton court, $U_0 = 117$ m s^{-1}, and the corresponding optimal initial angle $\theta^\star$ which verifies $(\partial x_0/\partial\theta_0)(U_{max}, \theta^\star) = 0$.

T (°C)	ρ (kg m^{-3})	$\mathcal{L}$ (m)	x_{max} (m)
0	1.293	4.60	13.1
10	1.247	4.77	13.5
20	1.204	4.94	13.9
30	1.164	5.11	14.3
40	1.127	5.28	14.7

The velocity of point C along the vectors $\mathbf{e}_{GC}$ and $\mathbf{e}_\varphi$ is:

$$\mathbf{U}_C = \begin{pmatrix} U\cos\varphi \\ -U\sin\varphi + l_{GC}\,\dot\varphi \end{pmatrix}. \tag{10}$$

Hence the angle φ satisfies the following equation:

$$(M_B l_{GB}^2 + M_C l_{GC}^2)\ddot\varphi \mathbf{e}_z = \mathbf{GB} \wedge \left(-\frac{1}{2}\rho S C_D U_B \mathbf{U}_B\right) + \mathbf{GC} \wedge \left(-\frac{1}{2}\rho s C_D U_C \mathbf{U}_C\right) \tag{11}$$

where $M_B l_{GB}^2 + M_C l_{GC}^2$ is the moment of inertia of the shuttlecock along the z direction. We have $\mathbf{GB} \wedge \mathbf{U}_B = l_{GB}(U\sin\varphi + l_{GB}\dot\varphi)\mathbf{e}_z$ and $\mathbf{GC} \wedge \mathbf{U}_C = l_{GC}(-U\sin\varphi + l_{GC}\dot\varphi)\mathbf{e}_z$, so that we can express equation (11) as:

$$(M_B l_{GB}^2 + M_C l_{GC}^2)\ddot\varphi = -\frac{1}{2}\rho S C_D U_B(U\sin\varphi + l_{GB}\dot\varphi) l_{GB} - \frac{1}{2}\rho s C_D U_C(-U\sin\varphi + l_{GC}\dot\varphi) l_{GC}. \tag{12}$$

Assuming that $U_B \simeq U_C \simeq U$, we get:

$$(M_B l_{GB}^2 + M_C l_{GC}^2)\ddot\varphi + \frac{\rho C_D}{2}(S\, l_{GB}^2 + s\, l_{GC}^2)U\dot\varphi + \frac{\rho C_D}{2}(S\, l_{GB} - s\, l_{GC})U^2\sin\varphi = 0. \tag{13}$$

As the point G is the center of mass of the two spheres placed in B and C of respective mass M_B and M_C, the distances l_{GB} and l_{GC} are linked by the relation $M_B l_{GB} = M_C l_{GC}$. Inserting the previous relation in equation (13) provides:

$$\ddot\varphi + \frac{\rho C_D}{2}\frac{S\frac{M_C}{M_B} + s\frac{M_B}{M_C}}{M_B + M_C}U\dot\varphi + \frac{\rho C_D}{2}\frac{SM_C - sM_B}{M_C\left(M_B + M_C\right)l_{GC}}U^2\sin\varphi = 0. \tag{14}$$

In the limit $SM_C \gg sM_B$, we obtain:

$$\ddot\varphi + \frac{\rho S C_D}{2M_B\left(1 + M_B/M_C\right)}U\dot\varphi + \frac{\rho S C_D U^2}{2\,M l_{GC}}\sin\varphi = 0 \tag{15}$$

where $M = M_C + M_B$. Equation (15) corresponds to (1) studied in this paper.

Appendix B

Badminton players always test shuttlecocks before competitions. They hit the projectile with a maximum strength from one extremity of the court. Only projectiles reaching the corridor on the opposite side are selected for the game. This test selects shuttlecocks which are appropriate to the current atmospheric conditions, and it proves that air temperature and humidity influence the trajectory.

The temperature modifies the shuttlecock aerodynamic length via air density ρ, as reported in table B1 . As air is hotter, the shuttlecock aerodynamic length increases. This implies an increase of the range of the projectile by about 10% between 10 and 40 °C, that is, in the typical range of temperature at which badminton is practised.

The effect of air humidity is less obvious to understand. At first glance, parameters in the aerodynamic length $\mathcal{L}$ do not depend on hygrometry. But such effects only occur with feather shuttlecocks. Goose feathers

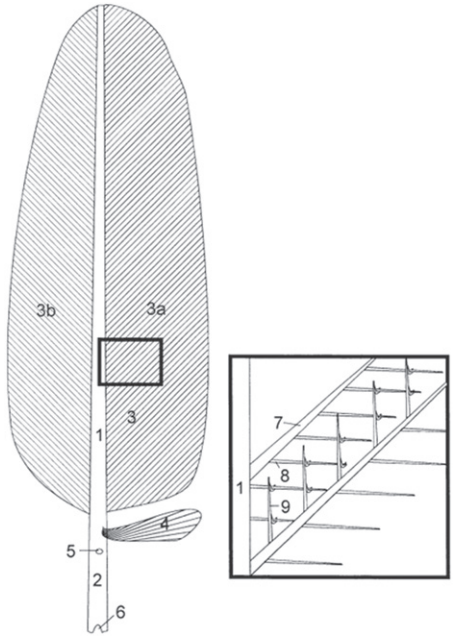

Figure B1. Sketch of a feather showing its microstructure. A typical feather features a main rod, called the rachis. Joined to the rachis are a series of branches, or barbs; the barbs themselves are also branched and form the barbules.

Table B2. Mass of a feathered shuttlecock as a function of air humidity. The aerodynamic length of the projectile is determined for $S = 28$ cm^2, $C_D = 0.6$ and $\rho = 1.2$ kg m^{-3}. The maximal range x_{max} is calculated for the maximal velocity recorded in a badminton court, $U_0 = 117$ m s^{-1}, and for the corresponding optimal initial angle $\theta^\star$ which verifies $(\partial x_0/\partial\theta_0)(U_{max}, \theta^\star) = 0$.

Relative humidity (%)	M (g)	$\mathcal{L}$ (m)	x_{max} (m)
15	5.20	5.16	14.4
32	5.30	5.25	14.6
42	5.33	5.29	14.7
92	5.51	5.46	15.1

possess structures at different scales (figure B1). Structures at the micro-scale are good precursors for small water droplets resulting from vapor condensation. This phenomenon explains why a feathered shuttlecock weight depends on air humidity, as does its aerodynamic length.

We conduct an experimental study of shuttlecock mass as a function of humidity conditions at $T = 20$ °C. Corresponding results are gathered in table B2 . These data reveal the increase of the weight of the projectile with air humidity up to 10%, which leads to increase the maximal range up to 5%.

This study proves that the shuttlecock aerodynamic length and its range increase with air temperature. Players usually counterbalance this effect by using lighter shuttlecocks when air is hotter. Alternatively, they do not hesitate to fold the extremities of feathers toward the interior or the exterior in order to modify the shuttlecock cross-section and adapt the aerodynamic length to the present atmospheric conditions. Also, players avoid aerodynamic length variation during a game by exposing the shuttlecocks to ambient humidity several hours before the game starts.

For clear strokes, the trajectory ends with a nearly vertical fall. This leads to a high sensitivity of the badminton game to wind. During vertical fall, wind blowing horizontally at a velocity U_w deviates the impacting point of the shuttlecock by a quantity $U_w^2 \sin^2\theta_0/g$. If $U_w = 1$ m s^{-1} (modest wind) and $\theta_0 = 60°$, the deviation is about 8 cm which is larger than the shuttlecock size. This explains why competitive badminton is always played indoors.

References

[1] Guillain J-Y 2002 *Histoire du Badminton* (Paris: Editions Publibook) pp 15–25
[2] Laffaye G 2013 *Comprendre et Progresser au Badminton* (Paris: Editions Chiron) p 61
[3] Cooke A J 2002 Computer simulation of shuttlecock trajectories *Sports Eng.* **5** 93–105
[4] Cooke A J 1999 Shuttlecock aerodynamics *Sports Eng.* **2** 85–96
[5] Alam F, Chowdhury H, Theppadungporn C and Subic A 2010 Measurements of aerodynamic properties of badminton shuttlecocks *Procedia Eng.* **2** 2487–92
[6] Chan C M and Rossmann J S 2012 Badminton shuttlecock aerodynamics: synthesizing experiment and theory *Sports Eng.* **15** 61–71
[7] Chen L M, Pan Y H and Chen Y J 2009 A study of shuttlecocks trajectory in badminton *J. Sports Sci. Med.* **8** 657–62
[8] Cohen C, Darbois-Texier B, Dupeux G, Brunel E, Quéré D and Clanet C 2014 The aerodynamic wall *Proc. R. Soc. A* **470** 20130497
[9] Lin C S, Chua C K and Yeo J H 2013 Turnover stability of shuttlecocks-transient angular response and impact deformation of feather and synthetic shuttlecocks *Procedia Eng.* **60** 106–11
[10] Etkin B and Reid L D 1982 *Dynamics of Flight: Stability and Control* (New York: Wiley)
[11] Phomsoupha M and Laffaye G 2014 Shuttlecock velocity during a smash stroke in badminton evolves linearly with skill level *Comput. Methods Biomech. Biomed. Eng.* **17** 140–1
[12] Hubbard M and Cooke A 1997 Spin dynamics of the badminton shuttlecock *6th Int. Symp. on Computer Simulation in Biomechanics* pp 42–43
[13] Kitta S, Hasegawa H, Murakami M and Obayashi S 2011 Aerodynamic properties of a shuttlecock with spin at high reynolds number *Procedia Eng.* **13** 271–7
[14] Darbois-Texier B, Cohen C, Dupeux G, Quéré D and Clanet C 2014 On the size of sports fields *New J. Phys.* **16** 033039
[15] Stubbs R 2011 *The Sports Book* (London: Dorling Kindersley)
[16] Tong Y M and Hong Y 2000 The playing pattern of world's top single badminton players (http://ojs.ub.uni-konstanz.de/cpa/article/download/2234/2090)
[17] Nielsen J N 1988 *Missile Aerodynamics* (Moffett Field, CA: NASA Ames Research Center)
[18] Sheldon J C and Burrows F M 1973 The dispersal effectiveness of the achene-pappus units of selected compositae in steady winds with convection *New Phytologist* **72** 665–75